π-Conjugated Polymers

DOI: 10.1002/anie.201205075

A Strategy for Revealing the Packing in Semicrystalline π-Conjugated Polymers: Crystal Structure of Bulk Poly-3-hexyl-thiophene (P3HT)**

*Dmytro Dudenko, Adam Kiersnowski, Jie Shu, Wojciech Pisula, Daniel Sebastiani, Hans Wolfgang Spiess, and Michael Ryan Hansen**

Polymers with extended π-conjugation and low band gaps are of broad scientific interest because of their promising applications as semiconductors in organic electronic devices. Examples include organic photovoltaic (OPV) cells, organic field-effect transistors (OFETs), and organic light-emitting diodes (OLEDs) with optimized properties toward light harvesting, charge-carrier mobility, and light emission, respectively.[1] Such polymers with lamellar π-stacks exhibit phase separation with regions of high and low order, that is, with crystalline and amorphous domains. This behavior is typically referred to as semicrystallinity, which is well known from polyolefins.[2] The specific organization of the macromolecules depends on the processing conditions.[3] Heterogeneous packing is also observed in photoconducting, columnar structures based on discotic aromatic compounds.[4] However, because the charge transport in such systems critically depends on the local packing,[5] structural details at the atomic level are of the utmost importance for material development. X-ray diffraction (XRD), which is well established in this area, requires high order, like that of single crystals. Even from a fiber diagram, only information about the relative assembly on a crystallographic lattice or chain-to-chain and π–π stacking distances can be derived.[6] Thus, a "multi-technique" approach is required to elucidate such structures.[7]

Recently, the combination of nuclear magnetic resonance (NMR) spectroscopy and quantum-chemical calculations of NMR properties, such as isotropic chemical shifts, J-couplings, and quadrupolar coupling parameters, has been established as a powerful approach to elucidate the structure of microcrystalline materials with atomic resolution,[8] often referred to as NMR crystallography.[9] In our study, we extend this approach to include XRD to handle semicrystalline polymers, for which single crystals are not available, placing emphasis on π-conjugated polymers. Our strategy is based on the use of XRD to assess long-range order from powder or fiber diagrams, and to employ high-resolution ^{1}H and ^{13}C solid-state NMR spectroscopy to acquire molecular constraints. The latter technique exploits the sensitivity of NMR spectroscopy toward local packing and conformations through ^{1}H and ^{13}C NMR chemical shifts and ^{1}H–^{1}H dipole–dipole couplings (DDCs).[10] Quantitative and specific packing information is obtained from quantum-chemical calculations of chemical shifts with the aid of nucleus-independent chemical shift (NICS) maps.[11] The NICS approach is particularly suited to quantify π–π stacking with ^{1}H NMR chemical shifts as a fingerprint of lamellar structures in polymers with extended π-conjugation. Specifically, we evaluated how the local magnetic fields are shielded (or deshielded) by neighboring chains within a stack. This evaluation enabled us to analyze the experimentally observed differences between solution- and solid-state ^{1}H NMR chemical shifts. Thus, we were able to identify packing models that are compatible with both the long- and short-range constraints, as obtained from XRD and solid-state NMR spectroscopy. Below, we demonstrate that a determination of the space group from XRD in combination with the spectroscopic and computational methods allowed us to fully determine the structure for such semicrystalline polymers.

In order to illustrate the potential of our strategy, we chose poly-3-hexyl-thiophene (P3HT) as a prominent example. It is one of the most frequently studied semiconducting polymers because of its widespread applications in organic electronic devices, resulting from its facile processability, high charge-carrier mobility (up to $0.1\,V\,cm^2\,s^{-1}$), and environmental stability.[12] P3HT is a semicrystalline polymer that consists of a π-conjugated backbone with head-to-tail arrangement of the polythiophene units and pendent alkyl side groups.[13] Three thermodynamically stable phases were reported for P3HT, termed phase I, II, and III. They are characterized by 3D crystalline order, 2D crystalline order with disordered side chains, and a layered phase of smectic symmetry, respectively.[13c] Herein, we focus on phase I of P3HT, because this is the thermodynamically stable phase that is observed after annealing. Therefore, phase I is the most relevant structure for organic electronics, in which annealing of the cast material is often performed.[14] We compare two P3HT samples with different molecular weights and regioregularities: P100 (Sepiolid™ P100, $M_W = 60.0\,kg\,mol^{-1}$,

[*] Dr. D. Dudenko, Dr. A. Kiersnowski, Dr. J. Shu, Dr. W. Pisula, Prof. Dr. D. Sebastiani, Prof. Dr. H. W. Spiess, Dr. M. R. Hansen
Max Planck Institute for Polymer Research
Ackermannweg 10, 55128 Mainz (Germany)
E-mail: mrh@mpip-mainz.mpg.de
Dr. A. Kiersnowski
Polymer Engineering and Technology Division
Wroclaw University of Technology
Wybrzeze Wyspianskiego 27, 50-370 Wroclaw (Poland)
Prof. Dr. D. Sebastiani
Institute of Chemistry—Physical Chemistry
Martin-Luther-University Halle-Wittenberg
06120 Halle/Saale (Germany)

[**] D.D. and J.S. thank the Max Planck Society for postdoctoral stipends. A.K. acknowledges the support from a Marie Curie Intra European Fellowship (PIEF-GA-2009-253521) granted within the 7th EU Framework Program.

Supporting information for this article is available on the WWW under http://dx.doi.org/10.1002/anie.201205075.

PDI = 2.2, regioregularity = 94%) and P200 (Sepiolid™ P200, M_W = 25.0 kg mol^{-1}, PDI = 1.6, regioregularity > 98%) obtained from BASF, Ludwigshafen.

Numerous XRD studies on P3HT provided insight into the crystalline structure of both bulk and thin-film samples, in addition to establishing relationships between molecular structure, packing, processing conditions, and charge-transport properties.[12a,15] P3HT in bulk and in thin films predominantly crystallizes in a monoclinic structure. Brinkmann and co-workers recently reported a space group of $P2_1/c$ along with unit-cell parameters a = 1.60 nm, b = 0.78 nm, c = 0.78 nm, and γ = 86.5° from electron diffraction on an epitaxially grown P3HT thin film.[16] However, the unit-cell parameters reported from XRD on bulk P3HT samples are somewhat smaller (a = 1.57 nm, b = 0.77 nm, c = 0.77 nm),[13c] thus indicating that structural parameters of epitaxially grown thin films may not be fully applicable to bulk P3HT. XRD of bulk polymers allows the analysis of the crystalline structure and the estimation of the phase composition at the same time. This is particularly important for P3HT, because recent studies of this polymer using NMR spectroscopy or differential scanning calorimetry (DSC) led to quite different degrees of crystallinities.[17]

To determine the unit-cell parameters and crystallinity for the two different P3HT samples, the diffractograms were deconvoluted into the individual contributions of amorphous and crystalline parts, as shown in Figures 1 and S1 (in the Supporting Information) for P100 and P200, respectively. The analysis gave a monoclinic unit cell with lattice constants of 0.76 nm, 0.77 nm, and 87° for b, c, and γ, respectively. The a-constants showed small differences for P100 and P200, with 1.63 and 1.64 nm for P100 and P200, respectively. This result is in agreement with previously reported values for P3HT with number-average molecular weights (M_n) ranging from 15 to 30 kg mol^{-1}.[15d] We attribute the small differences in a-constants for P100 and P200 to the difference in regioregularity (94% vs. > 98%), resulting in a different packing of hexyl side chains.[13c,18]

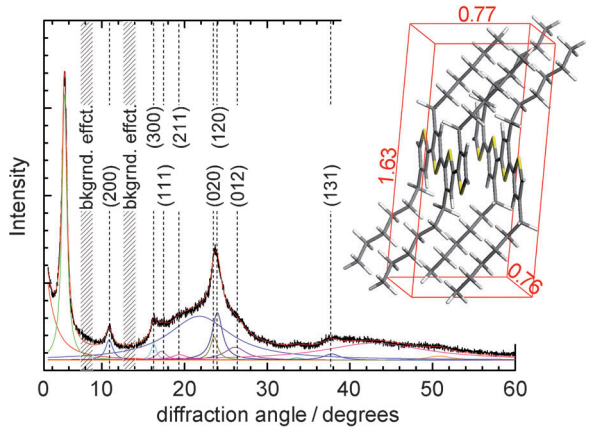

Figure 1. Powder X-ray diffractogram for P3HT (P100). The inset shows the derived monoclinic unit cell ($\alpha = \beta = 90°$, $\gamma = 87°$) with red numbers corresponding to the cell dimensions in nanometers. For further details see the Supporting Information.

In order to further characterize the packing in P100 and P200, we recorded small-angle X-ray scattering (SAXS) diagrams (see Figure S2). The absence of characteristic reflections in the SAXS curves suggests that as-synthesized P3HT adopts the form of nanowhiskers, as reported earlier.[19] Recrystallization of P100 from the melt led to a lamellar structure with a long spacing of about 14 nm (see Figure S2). In contrast, SAXS patterns recorded for P200 before and after melt-crystallization are identical. This indicates that recrystallization of P200 does not alter its nanostructure.

Figure 2 shows solid-state NMR spectra of P100 and P200. They include 2D homonuclear ^{1}H–^{1}H double-quantum/single-quantum (DQSQ) correlation spectra (Figure 2a and c), and 2D heteronuclear ^{13}C{^{1}H} frequency-switched Lee–Goldburg heteronuclear correlation (FSLG-HETCOR) spectra (Figure 2b and d) for measuring the spatial proximities of proton–proton and proton–carbon atoms.[20] In the former spectra, two intense ^{1}H NMR resonances are observed: a broad one centered at approximately 6.5 ppm (thiophene protons), and a second one centered at approximately 1.5 ppm (hexyl side chains). These signals are spatially close, as shown by the strong cross-correlation peaks located at both sides of the diagonal ($\delta_{DQ} \approx 8.0$ ppm). Moreover, the signal from the thiophene protons at around 6.5 ppm is split into two overlapping resonances that are centered at 6.9 and 6.0 ppm. Only the signal at 6.0 ppm displays an autocorrelation peak on the diagonal (see Figure 2a and c). In liquid-state NMR,

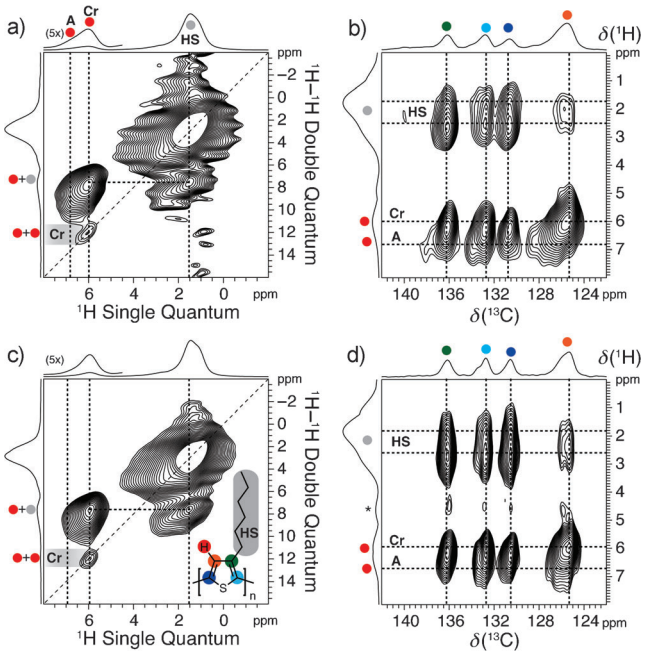

Figure 2. 2D ^{1}H–^{1}H DQSQ correlation and 2D ^{13}C{^{1}H} FSLG-HETCOR spectra for the two different P3HT samples, P100 (a, b) and P200 (c, d), recorded at 20.0 T using spinning frequencies of 15.0 and 25.0 kHz, respectively. a, c) One rotor period of BaBa recoupling was used. b, d) A cross-polarization time of 3.0 ms was employed. The labels **A**, **Cr**, and **HS** refer to amorphous, crystalline, and hexyl side chain, respectively. The asterisk in (d) indicates an artifact from the carrier frequency.

the thiophene protons resonate at $\delta_{iso} = 6.96$ (Figure S4). Thus, the weak signal at 6.9 ppm in the solid phase of P3HT is assigned to the amorphous fraction, which shows only limited, if any π–π stacking. However, the signal at 6.0 ppm in the solid phase of P3HT is shifted by 0.96 ppm to high field, which is characteristic of signals that are subjected to π–π stacking, and is assigned to π–π-stacked P3HT polymer chains in the crystalline regions. Furthermore, the autocorrelation peak for the signal at 6.0 ppm demonstrates that the thiophene protons in the crystalline fraction of P3HT have an internuclear distance below 4.0 Å.[21] This result indicates an intermolecular contact between adjacent layers of P3HT chains within a stack, because the shortest intramolecular distance between thiophene protons in regioregular P3HT is approximately 6.0 Å.

The semicrystalline nature of P3HT is best appreciated from the 2D $^{13}C\{^1H\}$ FSLG-HETCOR spectra in Figure 2b and d. Here, the ^{13}C NMR resonances from the crystalline regions appear as sharp resonances, while those from the amorphous fraction manifest themselves as shoulders to higher frequencies, most pronounced for the carbon site that bears the thiophene protons (labeled orange). This result illustrates that this position is particularly sensitive to local packing. Moreover, the ^{13}C resonances in the 2D $^{13}C\{^1H\}$ FSLG-HETCOR spectra are narrower for P200 than for P100. This observation shows that the local ordering of the polymer chains is higher in P200 with higher regioregularity, thus reducing defects in the π-conjugation along the P3HT polymer backbone.[22] These observations suggest that the specific regioregularity plays a role that is as important as the molecular weight with respect to the long-range charge-transport properties of P3HT.[23]

Next, we addressed the different kinds of crystallinity for P3HT, as deduced from XRD, NMR spectroscopy, and DSC. The analysis of the diffractograms allows the determination of relative crystallinity indexes (X_c^{XRD}) by comparing integral intensities of coherently scattered X-rays from the crystalline and amorphous parts (Figures 1 and S1). This comparison gives X_c^{XRD} values of 0.36 and 0.62 for P100 and P200, respectively. From solid-state NMR spectra, the crystallinity is obtained by deconvolution of ^1H magic-angle spinning (MAS) NMR spectra (Figure S5 and Table S3), giving X_c^{NMR} of 0.26 and 0.37 for P100 and P200, respectively. Interestingly, the crystallinity from DSC (X_c^{DSC}), determined for P100 and P200 from melting peaks in DSC traces (Figure S3) of 0.05 and 0.13, respectively, are much lower than X_c^{XRD} and X_c^{NMR}. This result suggests that the reported enthalpy of melting for P3HT of $\Delta H_m^{100} = 99\ J\ g^{-1}$ [19a] is most likely overestimated, as already noted by Pascui et al.,[17] and that further elucidation of the crystallization mechanism for P3HT should be considered. The crystallinities from XRD and NMR analyses also differ; the values from NMR spectroscopy are systematically lower than those from XRD. This is easily reconciled, as the X-ray reflections from the crystalline parts are much easier to quantify than the scattering from the amorphous regions.[24] X_c^{XRD} should be considered as the 3D crystallinity index, whereas X_c^{NMR} reflects the absolute degree of π–π stacking (1D) present in P3HT, a highly relevant parameter when addressing the charge-transport properties for P3HT. X_c^{NMR} is strongly related to how well the π-conjugated P3HT polymer backbones stack, how ordered the stacks are, and most importantly, how good the spatial overlap between neighboring P3HT chains is.[25]

To combine the molecular constraints from solid-state NMR spectroscopy and the unit-cell parameters from XRD, we performed ab initio molecular dynamic (MD) simulations and NICS map calculations under periodic boundary conditions (see the Supporting Information for details). These calculations take the dimensions of the monoclinic unit cell with five polythiophene layers for the periodic boundary conditions into account. Our model stacks were further simplified by truncating the hexyl side chains to methyl groups. Specific NICS maps were calculated for the position of the innermost thiophene layer. The three packing models considered for P3HT include the simple stacking of P3HT polymer chains (Figure 3a), displacement of every P3HT layer by one thiophene unit (Figure 3b), and flipping of every other layer (Figure 3c), corresponding to the symmetry operations of the space group $P2_1/c$.[26] The red and green arrows between thiophene protons in Figure 3 correspond to distances above or below 4 Å, respectively. Clearly, only the models presented in Figure 3a and c fulfill the distance constraint (< 4.0 Å), and the model in Figure 3c is favored because of its better space-filling properties for the hexyl side chains. A direct fingerprint of the packing organization in P3HT can be obtained from the NICS maps (Figure 3). These maps show that the ^1H NMR chemical shifts for the thiophene protons (marked by a dashed black circle) are shielded in the

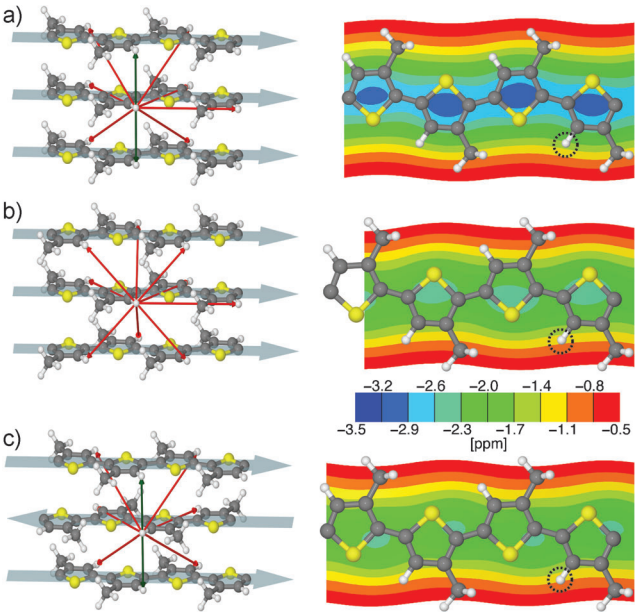

Figure 3. Packing models for P3HT considered in this work and their corresponding NICS maps. The NICS color bar quantifies the NMR chemical shift offset of the nuclei in a polymer chain induced by the electronic ring currents of all neighboring chains. Red and green arrows illustrate ^1H–^1H distances above and below 4.0 Å, respectively. The thiophene protons, marked by dashed black circles on the NICS maps, give rise to homonuclear correlation peaks if the internuclear distance is below 4.0 Å.

range from 1.1 to 1.6 ppm, depending on the packing structure. This observation demonstrates the strong sensitivity of the thiophene proton chemical shift toward the packing in P3HT, which again is in favor of the packing in Figure 3c. It is highly rewarding that the only model that fulfills both the distance constraint and the NICS map criteria is also the only structure that is consistent with the space group $P2_1/c$.

The final structure for phase I of P3HT is shown in Figures 4, S6a and b. It accommodates extended hexyl side chains, consistent with the $^{13}C\{^1H\}$ cross-polarization (CP)/

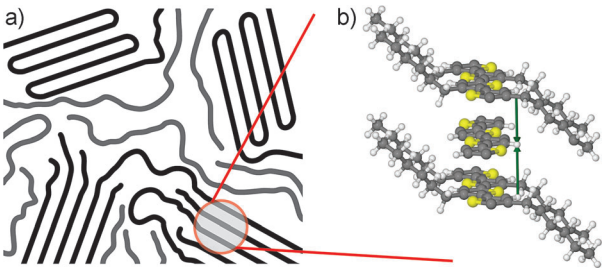

Figure 4. a) Schematic drawing of a semicrystalline polymer with regions of high (black) and low (grey) order. b) View along the stacked P3HT structure, illustrating the alternating packing of P3HT polymer chains. Green arrows indicate thiophene ^1H–^1H distances below 4 Å (Figure 2). For clarity, not all hexyl side chains are shown. Fractional atomic coordinates can be found in the Supporting Information.

MAS NMR spectra spectra (Figure S7), which show predominantly *trans* conformations. Moreover, it deviates from the structure derived for epitaxially grown P3HT thin films,[16] in which in particular the π–π stacking distances differ significantly, that is, 3.4 Å versus 3.9 Å determined here. The short stacking distance of 3.4 Å requires a 26° tilt of the P3HT backbones with respect to the *b*-axis, accompanied by a shift of 1.9 Å along the *c*-axis (see Figure 8 in Ref. [16]). Both of these structural features are absent in our structure (Figures 4 and S6), based on the observed ^1H NMR chemical shifts, which are particular sensitive to tilted π-stacks.[10b] NICS calculations for the epitaxial P3HT structure (see Figure S6c) show that the thiophene protons would then be shifted by 1.9 ppm to lower frequencies. This significant shift is not observed for bulk P3HT and large tilt angles can therefore be excluded. Thus, the differences between the two structures suggest that the packing of P3HT in epitaxially grown thin films might not represent that of the bulk structure. It remains to be seen, which of the two structures is present in P3HT:PCBM photovoltaic blends. Work along these lines is in progress.

In this work, we introduced a new systematic strategy for revealing the local packing in semicrystalline π-conjugated polymers. Our strategy takes advantages of a "multi-technique" approach, in which unit-cell parameters are derived from XRD, and molecular constraints are determined from solid-state NMR spectroscopy. The parameters derived from this strategy include the space group, that is, one of the first steps in a conventional approach to solve a crystal structure, distance constraints from ^1H double-quantum NMR, and chemical shifts. These experimental results are unified by quantum-chemical calculations, enabling the verification of specific packing models in silico and quantification of π-stacking effects. To introduce our strategy, we fully determined the bulk structure for phase I of P3HT, which crystallizes in the space group $P2_1/c$. Our approach can be compared with that employed for solution structures of biomacromolecules through distance constraints (NOE) and NMR chemical shifts.[27] This, however, requires a large number of NOE constraints, whereas in a crystalline solid, the periodicity described by the space group gives access to the full 3D structure from only a few constraints. Thus, our strategy, which we propose to term "multi-technique crystallography", can be applied in general to provide quantitative insights into the packing of semicrystalline polymers with specific intermolecular packing features, such as hydrogen bonds or stacking of aromatic moieties.

Received: June 28, 2012
Revised: July 26, 2012
Published online: October 4, 2012

Keywords: density-functional calculations · NMR spectroscopy · π-conjugated polymers · semiconductors · stacking interactions

[1] a) J. H. Burroughes, D. D. C. Bradley, A. R. Brown, R. N. Marks, K. Mackay, R. H. Friend, P. L. Burns, A. B. Holmes, *Nature* **1990**, *347*, 539–541; b) S. Günes, H. Neugebauer, N. S. Sariciftci, *Chem. Rev.* **2007**, *107*, 1324–1338; c) P. M. Beaujuge, J. M. J. Frechet, *J. Am. Chem. Soc.* **2011**, *133*, 20009–20029.

[2] G. R. Strobl, *The Physics of Polymers: Concepts for Understanding Their Structures and Behavior*, Springer, Heidelberg, **2007**.

[3] a) Y.-F. Yao, R. Graf, H. W. Spiess, D. R. Lippits, S. Rastogi, *Phys. Rev. E* **2007**, *76*, 060801; b) Y. Wei, R. Graf, J. C. Sworen, C.-Y. Cheng, C. R. Bowers, K. B. Wagener, H. W. Spiess, *Angew. Chem.* **2009**, *121*, 4687–4690; *Angew. Chem. Int. Ed.* **2009**, *48*, 4617–4620.

[4] a) M. R. Hansen, T. Schnitzler, W. Pisula, R. Graf, K. Müllen, H. W. Spiess, *Angew. Chem.* **2009**, *121*, 4691–4695; *Angew. Chem. Int. Ed.* **2009**, *48*, 4621–4624; b) M. R. Hansen, X. Feng, V. Macho, K. Müllen, H. W. Spiess, G. Floudas, *Phys. Rev. Lett.* **2011**, *107*, 257801.

[5] a) V. Coropceanu, J. Cornil, D. A. da Silva Filho, Y. Olivier, R. Silbey, J.-L. Bredas, *Chem. Rev.* **2007**, *107*, 926–952; b) X. Feng, V. Marcon, W. Pisula, M. R. Hansen, J. Kirkpatrick, F. Grozema, D. Andrienko, K. Kremer, K. Müllen, *Nat. Mater.* **2009**, *8*, 421–426.

[6] M. Möller, K. Matyjaszewski, *Polymer Science: A Comprehensive Reference*, *Vol. 2*, Elsevier, Amsterdam, **2012**.

[7] H. W. Spiess, *Macromolecules* **2010**, *43*, 5479–5491.

[8] a) R. K. Harris, *Solid State Sci.* **2004**, *6*, 1025–1037; b) F. Taulelle, *Solid State Sci.* **2004**, *6*, 1053–1057; c) B. Elena, L. Emsley, *J. Am. Chem. Soc.* **2005**, *127*, 9140–9146; d) M. R. Hansen, G. Madsen, H. J. Jakobsen, J. Skibsted, *J. Phys. Chem. A* **2005**, *109*, 1989–1997; e) A. L. Webber, L. Emsley, R. M. Claramunt, S. P. Brown, *J. Phys. Chem. A* **2010**, *114*, 10435–10442; f) L. Mafra, S. M. Santos, R. Siegel, I. Alves, F. A. Almeida Paz, D. Dudenko, H. W. Spiess, *J. Am. Chem. Soc.* **2012**, *134*, 71–74.

[9] R. K. Harris, R. E. Wasylishen, M. J. Duer, *NMR Crystallography*, Wiley, Weinheim, **2009**.

[10] a) S. P. Brown, H. W. Spiess, *Chem. Rev.* **2001**, *101*, 4125–4155; b) C. Ochsenfeld, S. P. Brown, I. Schnell, J. Gauss, H. W. Spiess,

J. Am. Chem. Soc. **2001**, *123*, 2597 – 2606; c) M. Fritzsche, A. Bohle, D. Dudenko, U. Baumeister, D. Sebastiani, H. W. Spiess, M. R. Hansen, S. Höger, *Angew. Chem.* **2011**, *123*, 3086 – 3089; *Angew. Chem. Int. Ed.* **2011**, *50*, 3030 – 3033.

[11] a) P. V. R. Schleyer, C. Maerker, A. Dransfeld, H. Jiao, N. Hommes, *J. Am. Chem. Soc.* **1996**, *118*, 6317 – 6318; b) D. Sebastiani, *ChemPhysChem* **2006**, *7*, 164 – 175.

[12] a) H. Sirringhaus, P. Brown, R. H. Friend, M. Nielsen, K. Bechgaard, B. Langeveld-Voss, A. Spiering, R. A. J. Janssen, E. W. Meijer, P. Herwig, D. de Leeuw, *Nature* **1999**, *401*, 685 – 688; b) C. Goh, R. J. Kline, M. D. McGehee, E. N. Kadnikova, J. M. J. Frechet, *Appl. Phys. Lett.* **2005**, *86*, 122110.

[13] a) S. Hugger, R. Thomann, T. Heinzel, T. Thurn-Albrecht, *Colloid Polym. Sci.* **2004**, *282*, 932 – 938; b) M. Brinkmann, J. C. Wittmann, *Adv. Mater.* **2006**, *18*, 860 – 863; c) Z. Wu, A. Petzold, T. Henze, T. Thurn-Albrecht, R. H. Lohwasser, M. Sommer, M. Thelakkat, *Macromolecules* **2010**, *43*, 4646 – 4653.

[14] a) A. Zen, J. Pflaum, S. Hirschmann, W. Zhuang, F. Jaiser, U. Asawapirom, J. P. Rabe, U. Scherf, D. Neher, *Adv. Funct. Mater.* **2004**, *14*, 757 – 764; b) K. Inoue, R. Ulbricht, P. C. Madakasira, W. M. Sampson, S. Lee, J. Gutierrez, J. Ferraris, A. A. Zakhidov, *Synth. Met.* **2005**, *154*, 41 – 44.

[15] a) M. J. Winokur, D. Spiegel, Y. Kim, S. Hotta, A. J. Heeger, *Synth. Met.* **1989**, *28*, 419 – 426; b) T. Prosa, M. Winokur, J. Moulton, P. Smith, A. J. Heeger, *Macromolecules* **1992**, *25*, 4364 – 4372; c) R. J. Kline, M. D. McGehee, E. N. Kadnikova, J. S. Liu, J. M. J. Frechet, *Adv. Mater.* **2003**, *15*, 1519 – 1522; d) M. Brinkmann, *J. Polym. Sci. Part B* **2011**, *49*, 1218 – 1233.

[16] N. Kayunkid, S. Uttiya, M. Brinkmann, *Macromolecules* **2010**, *43*, 4961 – 4967.

[17] O. F. Pascui, R. Lohwasser, M. Sommer, M. Thelakkat, T. Thurn-Albrecht, K. Saalwächter, *Macromolecules* **2010**, *43*, 9401 – 9410.

[18] E. Mena-Osteritz, A. Meyer, B. Langeveld-Voss, R. A. J. Janssen, E. W. Meijer, P. Bäuerle, *Angew. Chem.* **2000**, *112*, 2791 – 2796; *Angew. Chem. Int. Ed.* **2000**, *39*, 2679 – 2684.

[19] a) S. Malik, A. K. Nandi, *J. Polym. Sci. Part B* **2002**, *40*, 2073 – 2085; b) C.-Y. Chen, S.-H. Chan, J.-Y. Li, K.-H. Wu, H.-L. Chen, J.-H. Chen, W.-Y. Huang, S.-A. Chen, *Macromolecules* **2010**, *43*, 7305 – 7311.

[20] a) B. J. van Rossum, H. Forster, H. J. M. deGroot, *J. Magn. Reson.* **1997**, *124*, 516 – 519; b) M. Feike, D. E. Demco, R. Graf, J. Gottwald, S. Hafner, H. W. Spiess, *J. Magn. Reson. Ser. A* **1996**, *122*, 214 – 221.

[21] I. Schnell, H. W. Spiess, *J. Magn. Reson.* **2001**, *151*, 153 – 227.

[22] P. Kohn, S. Huettner, H. Komber, V. Senkovskyy, R. Tkachov, A. Kiriy, R. H. Friend, U. Steiner, W. T. S. Huck, J.-U. Sommer, M. Sommer, *J. Am. Chem. Soc.* **2012**, *134*, 4790 – 4805.

[23] a) R. J. Kline, M. D. McGehee, E. N. Kadnikova, J. S. Liu, J. M. J. Frechet, M. F. Toney, *Macromolecules* **2005**, *38*, 3312 – 3319; b) R. J. Kline, M. D. McGehee, *Polym. Rev.* **2006**, *46*, 27 – 45.

[24] N. Stribeck, *X-ray Scattering of Soft Matter*, Springer, Berlin, **2007**.

[25] J. Nelson, J. J. Kwiatkowski, J. Kirkpatrick, J. M. Frost, *Acc. Chem. Res.* **2009**, *42*, 1768 – 1778.

[26] T. Hahn, *International Tables of Crystallography*, *Vol. A*, 5th ed., **2005**.

[27] K. Wüthrich, *Angew. Chem.* **2003**, *115*, 3462 – 3486; *Angew. Chem. Int. Ed.* **2003**, *42*, 3340 – 3363.

